Determination of dipole and quadrupole polarizabilities of Mg^+ by fine-structure measurements in high-L $n=17$ Rydberg states of magnesium

E. L. Snow
Department of Physics, SUNY Fredonia, Fredonia, New York 14063, USA

S. R. Lundeen
Department of Physics, Colorado State University, Fort Collins, Colorado 80523, USA

(Received 14 March 2008; published 8 May 2008)

Fine-structure intervals between $n=17$ Rydberg states of magnesium with $6 \leq L \geq 11$ were measured using the resonant excitation Stark ionization spectroscopy technique. Comparing the measured intervals with the long-range polarization model determines the dipole and quadrupole polarizabilities of Mg^+ to be $\alpha_1 = 35.00(5) a_0^3$ and $\alpha_2 = 222(54) a_0^5$, respectively.

DOI: 10.1103/PhysRevA.77.052501 PACS number(s): 32.10.Dk, 32.10.Fn

I. INTRODUCTION

The interaction between a nonpenetrating high-L Rydberg electron and a positive ion core with $L=0$ creates a fine-structure pattern approximately proportional to the polarizability of the ion core. Measurements of such fine-structure patterns provide information about the dipole and quadrupole polarizability of the positive ion core. In order to extract this information, measurements must be obtained across as wide a range of L's as possible, in states where core penetration can be neglected and nonadiabatic effects are small. The RESIS method provides convenient experimental access to such states in Rydberg atoms, molecules, and ions [1]. The desired Rydberg levels are prepared by charge exchange between an accelerated ion beam and a laser-excited Rydberg target, and detected by excitation with a Doppler-tuned CO_2 laser followed by Stark ionization. In the present work, the RESIS technique was used to detect microwave induced transitions between $n=17$ levels of Mg with $6 \leq L \leq 11$. The measured intervals conform closely to the pattern predicted by the long-range polarization model. Comparison with this model leads to a precise determination of the dipole polarizability of Mg^+ and the first measurement of that ion's quadrupole polarizability.

Nonpenetrating Rydberg states of Mg were first observed in the solar emission spectrum. Chang and Noyes [2] identified ten lines obtained with high resolution Fourier transform spectroscopy as belonging to the $(n,n')=(8,7)$, (7,6), (6,5), and (9,7) series, usually with the highest possible values of L. The identification rested on solar abundances, theoretical calculations of the dipole polarizability of Mg^+, and a simple polarization model of the intervals. Best agreement with the observed intervals was obtained if the polarizability, α_1, was taken to be 33.6 a_0^3, in acceptable agreement with theoretical estimates. Later, Lyons and Gallagher measured *nf-ng*, *nf-ni*, and *nf-nh* intervals in Mg, using stepwise laser excitation and multiphoton microwave spectroscopy [3]. By analysis of the *g-h* and *h-i* intervals, which were assumed to correspond to nonpenetrating states, they determined $\alpha_1 = 33.8(5) a_0^3$. More recently, there have been considerable improvements both in the theoretical calculations of ion properties and in the theoretical models that relate observed fine-structure patterns to the ion polarizability. Relativistic many-body calculations of properties of atoms and ions with a single valence electron outside a closed shell have received special attention because of the connection to parity nonconserving interactions in atomic systems, and the resulting need to use calculated atomic matrix elements at the 0.1% level of precision to extract information about fundamental interactions from experimental measurements [4,5]. Since Mg^+ is an example of such an ion, measurements of any of its properties, such as lifetimes and polarizabilities, at or near the 0.1% level, provide valuable tests of these improving calculations. One area of progress with regard to the theoretical models of high-L fine-structure patterns is improved understanding of the influence of nonadiabatic effects, both on the fine-structure patterns and on the energy splittings due to electron spin. These are illustrated in recent studies of barium Rydberg fine structure [6]. Another development is appreciation of the influence of higher order terms in the polarization potential, proportional to r^{-7} and $L(L+1)r^{-8}$, which can significantly alter the apparent slope of the polarization plots, complicating efforts to extract reliable values of the quadrupole polarizability, α_2, from experimental data. Consideration of these effects altered the value of α_2 extracted from recent measurements in barium by a factor of 2, giving good agreement with theoretical calculations [6]. Taken together, these developments motivate improved measurements of fine-structure patterns in magnesium.

II. EXPERIMENT

Observations of fine-structure intervals in the $n=17$ state of a magnesium optical transition were obtained by microwave RESIS techniques. The schematic of the apparatus is shown in Fig. 1 with an exaggerated energy level diagram below it to show an example of the corresponding selective laser excitation and microwave transitions that occur in each interaction region. This is the same apparatus and technique previously used in measurements of barium [6]. A fast neutral magnesium beam with a population distribution centered about $n=9$ and consisting of all possible angular momentum states was created by single electron capture by a 9.5 keV Mg^+ ion beam from a Rydberg target [7]. The fast ion beam

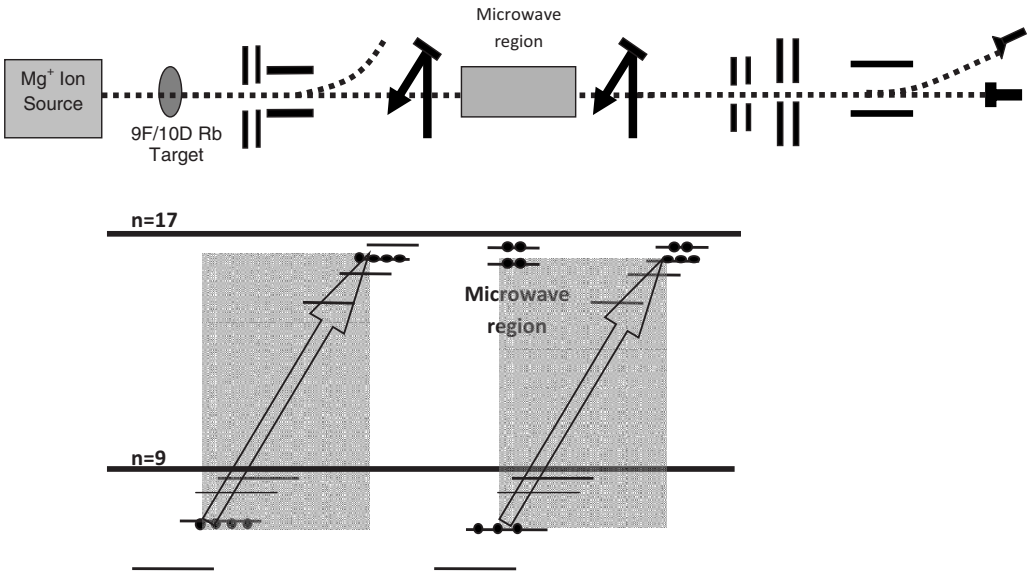

FIG. 1. Schematic diagram of microwave RESIS apparatus used for this study. An ion beam is created in a Colutron model-101 ion source. The ions are then collided with a selectively excited $9F/10D$ Rb target where some ions capture an electron. States of $n=15$ and higher are then Stark ionized in the pre-ionizer and deflected with the remaining Mg^+ ions to be collected in a Faraday cup. Neutral magnesium atoms with $n<15$ enter the first CO_2 laser interaction region. Here a Doppler-tuned CO_2 laser excites the $n=9$ atoms to $n=17$, depicted as the first arrow in the diagram of the energy levels below the apparatus schematic. Let each circle represent 1000 atoms residing in the energy level they are overlapping, so after the first laser region there is an equal population of 4000 atoms in the $n=9$, $L=6$ and the $n=17$, $L=7$ states. The microwave region can then excite a transition within the $n=17$ upper state, splitting the upper state population equally between the $L=7$ and 8 states. The second laser interaction region then repopulates the initial upper state if a microwave transition has occurred, as shown by the second large arrow and a population of 3000 atoms in the $n=9$, $L=6$ and $n=17$, $L=7$ levels. The excited states are then Stark ionized in the stripper and focused by the lens and the resulting signal ions are detected on a channeltron electron multiplier. A total current of 5000 ions is found if the microwave transition occurs, but only 4000 ions if it does not. The measured signal, the change in ion current caused by the microwaves, is 1000 ions in this case.

was produced in a Colutron model 101 ion source and a velocity filter was used to select the Mg^+ beam. The Rydberg target is a thermal Rb beam that is stepwise excited by three New Focus Vortex diode lasers to the $9F/10D$ state. Depending on target and beam conditions about 1% neutralization occurs in the Rydberg target. Upward excitations of the $n=9$ high-L states in the neutral beam to the $n=17$ upper states are produced by a CO_2 laser, operating on the $10R$ (20) transition at 975.9304 cm^{-1}, which is Doppler-tuned by changing the angle of intersection between the laser beam and the fast Rydberg beam. The transitions needed for this study, corresponding to excitation from $n=9$ to $n=17$ levels with $L=6$, 7, 8, and 9 are completely resolved. The detector consists of a Stark ionization region, which ionizes all population with $n\geq 17$, and bends the resulting charged beam onto a channel electron multiplier. In order to reduce the background due to initial upper Rydberg state population created in charge capture, all states with $n>15$ are Stark ionized and deflected out of the beam path by a strong electric field immediately following the Rydberg target.

In order to detect microwave transitions between $n=17$ levels, a microwave region and a second laser region are added, as in Fig. 1. The first laser region saturates the upward transition into a specific $n=17$ level, equalizing the populations of the $(9, L-1)$ and $(17, L)$ levels. If the microwave frequency matches the interval separating the $(17, L)$ and $(17, L\pm 1)$ levels, population will be transferred out of the $(17, L)$ level, allowing the second laser region, set to the same Doppler-tuned frequency as the first region, to excite additional atoms into the $(17, L)$ level. Thus the combination of the two laser regions and the microwave region excites a larger number of atoms into the $n=17$ level when a microwave transition occurs. The measured signal is the Stark ionized ion current synchronous with the 300 Hz amplitude modulation of the microwave field. It reveals a resonance peak when a microwave transition in the upper state occurs. In this study, all transitions were electric-dipole allowed $\Delta L=1$ transitions except for one two-photon $\Delta L=2$ transition that was used to locate the $L=11$ level.

The microwave interaction regions used are eccentric coaxial transmission lines excited by a traveling wave that propagates either co- or counterpropagating to the Rydberg beam. The microwave field is produced by a microwave frequency synthesizer. The microwave regions were shielded from motional fields due to the Earth's magnetic field by two

TABLE I. Mg $n=17$ fine-structure intervals.

$n=17$, $L-L'$	No. of observations	ΔE_{Obs} (MHz)
6–7	6	1520.809(15)
7–8	7	669.588(20)
8–9	6	324.044(45)
9–10	5	168.806(42)
*9–11	4	262.223(75)

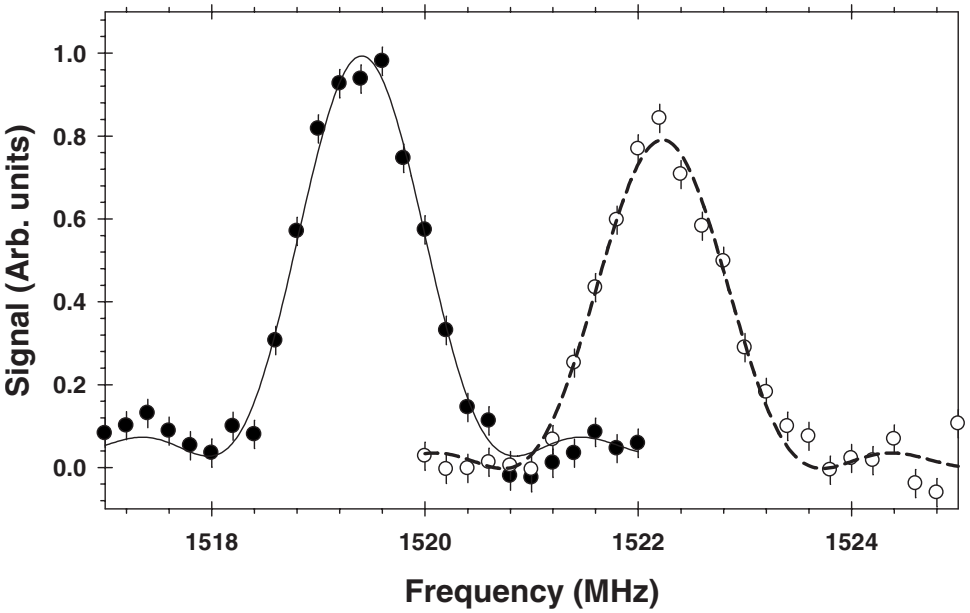

FIG. 2. The Mg $n=17$ $L=6$ to 7 microwave transition observed both co- and counterpropagating. The straight average of the fitted line centers will give the Doppler-free transition frequency.

layers of μ metal. Figure 2 shows a scan for both directions of propagation for microwave RESIS signals of magnesium $n=17$, $L=6$ to $n'=17$, $L'=7$. Fits of the microwave signals provide the transition line centers. The observed linewidths were approximately 1 MHz, due mostly to the transit time through the microwave interaction regions. No evidence was seen of spin splittings due to the interactions with either core or Rydberg spins, which are predicted to be less than 0.3 MHz. This is in contrast to observations in barium, where interactions with the core spin produce very large effects, but is in agreement with the model that reconciles similar effects in Si III, barium, and helium [8]. The Doppler-free interval is taken to be the average of the fitted centers for the two directions of propagation. Each transition frequency was measured at least four times, and the uncertainty associated with the average result was determined from the scatter of the repeated measurements. Table I summarizes the measured fine-structure intervals. A small ac Stark shift correction was applied to the line center of the two-photon interval. The calculated ac Stark shift for the magnesium $n=17$, $L=9$ to 11 interval is 0.105(20) MHz for the microwave region in which it was observed.

III. ANALYSIS

The energy of a particular Rydberg level can be expressed as

$$E(n,L) = E^{[0]}(n) + E_{\mathrm{rel}}(n,L) + \langle nL|V_{\mathrm{eff}}|nL\rangle + \sum \frac{|\langle nL|V_{\mathrm{eff}}|n'L'\rangle|^2}{[E^{[0]}(n) - E^{[0]}(n')]} \quad (1)$$

where $E^{[0]}$ is the hydrogenic energy, and the second term is the hydrogenic relativistic contribution. The third and dominant term is the expectation value of the effective potential, V_{eff},

$$V_{\mathrm{eff}}(r) = -\frac{C_4}{r^4} - \frac{C_6}{r^6} - \frac{C_7}{r^7} - C_{8L}\frac{L(L+1)}{r^8} - \frac{C_8}{r^8} + \cdots, \quad (2)$$

where each coefficient C_i is a property of the free ion core [9]. The fourth term of Eq. (1) is referred to here as the effective second order energy contribution, E_{sec}. This represents the contribution to the Rydberg state energy due to coupling between different Rydberg series. As long as these energy shifts are small, which is the case here, they can be

TABLE II. Summary of the corrections and scaling of the measured fine-structure intervals. The relativistic and effective second order energy contributions are given in columns 3 and 4. Column 5 gives the calculated Stark shift rate, κ, of the observed transition. Also listed are the calculated ratios of expectation value differences for the corresponding transitions and the ratio of the corrected energy (in a.u.) to the difference in expectation values of r^{-4} in the two levels. Energies are given in MHz.

$nL-n'L'$	ΔE_{Obs}	ΔE_{rel}	ΔE_{Sec}	κ [MHz/(V/cm)^2]	$\Delta\langle r^{-6}\rangle/\Delta\langle r^{-4}\rangle$	$\Delta E_{\mathrm{Corr}}/\Delta\langle r^{-4}\rangle$
17,6–17,7	1520.809(15)	0.732	7.49(32)	−17.8	0.002523	17.0419(36)
17,7–17,8	669.588(20)	0.560	1.436(30)	−27.0	0.001363	17.2369(9)
17,8–17,9	324.044(45)	0.442	0.331(3)	−36.8	0.000794	17.3347(24)
17,9–17,10	168.806(42)	0.358	0.087(1)	−43.2	0.000489	17.3723(43)
*17,10–17,11	93.417(86)	0.296	0.027(0)	−48.2	0.000313	17.394(16)

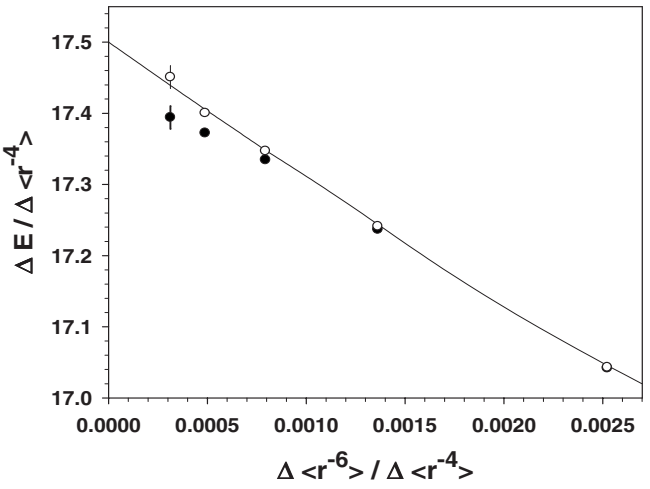

FIG. 3. Magnesium polarization plot, where the corrected line centers normalized to $\Delta\langle r^{-4}\rangle$ are plotted vs $\Delta\langle r^{-6}\rangle/\Delta\langle r^{-4}\rangle$. The solid data points are the normalized corrected fine-structure intervals, from Table II. The hollow points have been corrected for the stray dc electric field Stark shifts using the fitted value of B_E from Eq. (3). The solid line illustrates the fit to the data, including only the first three terms of Eq. (3).

calculated using the same effective potential, V_{eff}, whose expectation value is the dominant source of the fine-structure pattern. In order to simplify the interpretation of the measured fine-structure intervals, the small contributions from E_{rel} and E_{sec} are calculated and subtracted from the measured intervals, giving corrected intervals that can be considered to be equivalent to a simple expectation value of V_{eff}. The calculated corrections are shown in columns 3 and 4 of Table II. The effective second order contributions, ΔE_{sec}, are estimated from the first term proportional to $(C_4)^2$, using an expression calculated by Drake [10], and a separate calculation of the second term proportional to C_4C_6. The uncertainty in the ΔE_{sec} correction is taken to be half the size of the C_4C_6 term plus 0.5% of the $(C_4)^2$ term.

From these corrected intervals the two leading ion core properties, C_4 and C_6, can be extracted. If only these first two terms contribute significantly to the fine structure, the corrected intervals, normalized to $\Delta\langle r^{-4}\rangle$, would be expected to form a straight line when plotted vs the ratio of $\Delta\langle r^{-6}\rangle$ to $\Delta\langle r^{-4}\rangle$. Table II shows the scaled intervals and this ratio. The relevant expectation values are computed assuming hydrogenic radial functions, with proper scaling to account for the core mass. Figure 3 illustrates such a plot, and shows that it is indeed approximately linear. Some nonlinearity is evident in the highest L intervals, at the left in Fig. 3, due to the increasing sensitivity of those intervals to small stray fields in the microwave region. The presence of a small field ($\leq$0.1 V/cm) was independently indicated by a comparison of $L=7$ to $L=8$ and $L=8$ to $L=9$ intervals $n=20$ and $n=17$, which differ by about a factor of 5 in their sensitivity to stray fields. Because the measured intervals appeared to be consistent from day to day, we choose to account for the Stark shifts by including a term in the fit of the data that is proportional to the calculated Stark shift of each interval, which are tabulated in Table II. The fit indicates an average stray field of 0.08(2) V/cm. Including a term in the fit proportional to $\Delta\langle r^{-8}\rangle/\Delta\langle r^{-4}\rangle$ allows for the possibility of some curvature in the data pattern due to the C_8 term in V_{eff}. Although curvature of this type, which would be most pronounced in the lower L intervals at the right in Fig. 3, is not evident there, including this term in the fit is important to avoid underestimating the uncertainty in the slope of the plot. So, in summary, the scaled intervals listed in Table II are fit by

$$\frac{\Delta E_{\text{Corr}}}{\Delta\langle r^{-4}\rangle} = B_4 + B_6\left[\frac{\Delta\langle r^{-6}\rangle}{\Delta\langle r^{-4}\rangle}\right] + B_8\left[\frac{\Delta\langle r^{-8}\rangle}{\Delta\langle r^{-4}\rangle}\right] + B_E\frac{\kappa}{\Delta\langle r^{-4}\rangle}, \tag{3}$$

where B_E is the stray electric field squared. The fitted parameters were found to be

$$B_4 = 17.499(24),$$

$$B_6 = -198(23),$$

$$B_8 = 5600(4900),$$

$$B_E = 0.0063(34).$$

The traditional interpretation of the parameters is as follows: the intercept, B_4, is simply $C_4=\alpha_1/2$, and the slope, B_6, is equal to $C_6=(\alpha_2-6\beta_1)/2$. However, as seen in similar systems of barium [6] and Si^{2+} [11], higher order terms proportional to r^{-7} and $L(L+1)r^{-8}$ may alter this interpretation. These terms have a dependence on L that is intermediate between r^{-6} and r^{-8}, but they cannot be distinguished from a linear combination of r^{-4}, r^{-6}, and r^{-8}. Therefore if they are present they can affect the fitted slope, B_6, and invalidate its simple interpretation [9].

The coefficients, C_7 and C_{8L}, have been formally calculated [9], and their magnitudes can be estimated under the simplifying assumption that only the lowest P state and the lowest D state in Mg^+ contribute to the sum over states occurring in these coefficients. This approximation is supported by the dominance of the oscillator strengths of those transitions. Even with this approximation, numerical estimates of C_7 and C_{8L} requires calculations of a small number of matrix elements that do not occur in the coefficients, α_1, α_2, and β_1. The theoretical matrix elements used in these calculations are given in Table III. The necessary calculations were carried out by others using relativistic all-order methods [12,13], giving the following estimates: $C_7=-1684(19)$ and

TABLE III. Calculated matrix elements of the dipole and quadrupole transition strengths and excitation energies used to estimate the values of the C_7 and C_8 coefficients [12,13].

Matrix element	Value (a.u.)	ΔE (a.u.)
$\langle 3S\|\vec{D}\|3P\rangle$	2.90	0.16280
$\langle 3P\|\vec{D}\|3D\rangle$	5.10	N/A
$\langle 3S\|\vec{\vec{Q}}\|3D\rangle$	11.04	0.32573
$\langle 3P\|\vec{\vec{Q}}\|3P\rangle$	−15.08	N/A

TABLE IV. Estimation of the influence of the higher order terms in V_{eff} proportional to C_7 and C_{8L} on the interpretation of the intercept (B_4) and slope (B_6) of the polarization plot of Fig. 3. The theoretical estimates for these coefficients are given in column 2 and the fit parameters from the expression given in Eq. (4) of the text are shown in columns 3–5. The final two columns give the resulting adjustment to the intercept and slope of the polarization plot. Values are given in atomic units.

Term	C_i	A_1	A_2	A_3	ΔB_4	ΔB_6
$\Delta\langle r^{-7}\rangle/\Delta\langle r^{-4}\rangle$	−1684(19)	-3.77×10^{-6}	0.0267	9.3	0.0063(1)	−44.96(51)
$\Delta[L(L+1)\langle r^{-8}\rangle]/\Delta\langle r^{-4}\rangle$	1170(12)	-6.91×10^{-6}	0.0460	25.7	−0.0081(1)	53.82(55)

$C_{8L}=1170(12)$. The uncertainties in these estimates are derived from an assumed uncertainty of 0.5% in each calculated matrix element, but are large enough to also include uncertainty due to inclusion of only the lowest core P and D states. The necessary excitation energies are well known [14].

The parametrization of the smooth functions $\Delta\langle r^{-7}\rangle/\Delta\langle r^{-4}\rangle$ and $\Delta[L(L+1)\langle r^{-8}\rangle]/\Delta\langle r^{-4}\rangle$ vs $\Delta\langle r^{-6}\rangle/\Delta\langle r^{-4}\rangle$ were obtained by fitting each to the following expression:

$$A_1 + A_2\left[\frac{\Delta\langle r^{-6}\rangle}{\Delta\langle r^{-4}\rangle}\right] + A_3\left[\frac{\Delta\langle r^{-8}\rangle}{\Delta\langle r^{-4}\rangle}\right]. \tag{4}$$

The values of $\Delta\langle r^{-7}\rangle/\Delta\langle r^{-4}\rangle$ and $\Delta[L(L+1)\langle r^{-8}\rangle]/\Delta\langle r^{-4}\rangle$ are calculated for each of the observed transitions and fit to Eq. (4) with weights identical to that of the corresponding observed energy intervals. The parameters determined by the fit indicate the magnitude at which the C_7 and C_{8L} terms contribute to the intercept and initial slope of this magnesium polarization plot. Table IV gives the estimated coefficients, C_7 and C_{8L}, and the fitted parameters, A_1, A_2, and A_3 for each case. Together, these indicate the degree to which the fitted coefficients B_i differ from the corresponding coefficients in V_{eff}, C_i,

$$C_4 = B_4 - \Delta B_4 = B_4 - C_7 A_1^7 - C_{8L} A_1^{8L},$$

$$C_6 = B_6 - \Delta B_6 = B_6 - C_7 A_2^7 - C_{8L} A_2^{8L}. \tag{5}$$

In the case of the intercept C_4, the correction $\Delta B_4 = -0.0018(2)$, which is very small compared to the experimental uncertainty. For the slope of the polarization plot, C_6, the estimated correction is $\Delta B_6 = 9(1)$, producing a marginally significant modification of the interpretation of the fit coefficient B_6.

The dipole polarizability of Mg^+ is twice C_4, or $\alpha_1 = 35.00(5)a_0^3$. This is an order of magnitude more precise than the previous measurement from Rydberg fine structure [3]. It is also a factor of 5 more precise, and in good agreement with the value, $34.62(26)a_0^3$ deduced by Theodosiou *et al.* from a 1% measurement of the Mg^+ $3p$ radiative lifetime [15]. As pointed out by Curtis, the precise polarizability measurement could now be used to improve the precision of the $3p$ lifetime [16]. For comparison, some recent theoretical calculations of α_1 are listed in Table V. The two most recent calculations are in very good agreement with our measurement.

Since $2C_6 = \alpha_2 - 6\beta_1$, determining the quadrupole polarizability α_2 from the coefficient C_6 requires independent evaluation of β_1, the first nonadiabatic correction to the dipole polarizability. A very simple estimate can be made by assuming that only the $3p$ state contributes to the polarizability. In this approximation,

$$\beta_1 \cong \frac{\alpha_1}{2E(3p)} = 107a_o^5. \tag{6}$$

A more precise estimate with a rigorous error bound can be found by considering the contributions of higher p states to β_1, and taking into consideration the sum rule satisfied by the oscillator strengths in this series [16]. The result of that estimate is $\beta_1 = 106(1)a_0^5$ [17]. Using this value of β_1 and the experimentally determined value, $C_6 = -207(24)$a.u., the quadrupole polarizability of Mg^+ is determined, $\alpha_2 = 222(54)a_0^5$. This is somewhat larger than the recent calculations, shown in Table V, but differs by less than two standard deviations.

TABLE V. Current and previous experimental values along with theoretical calculations of the dipole and quadrupole polarizabilities of Mg^+ given in atomic units.

	This work	Previous reports	Theory
α_1	35.00(5)	33.6,[a] 33.80(50),[b] 34.62(26)[c]	35.01,[d] 35.66,[e] 35.01,[f] 34.14[c]
α_2	222(54)		156,[d] 156.1[f]

[a]Chang and Noyes, Ref. [2].
[b]Lyons and Gallagher, Ref. [3].
[c]Theodosiou, *et al.*, Ref. [15].
[d]Safronova, Ref. [13].
[e]Hamonou and Hibbert, Ref. [18].
[f]Mitroy and Zhang, Ref. [19].

IV. CONCLUSION

Measurements of the fine-structure pattern in high-L $n=17$ Rydberg states of Mg have been extended to much higher L than previous measurements. The extended data pattern provides a more precise value for the dipole polarizability of Mg^+ and the first measurement of its quadrupole polarizability. The influence of higher-order terms in the effective potential, proportional to C_7 and C_{8L}, was considered in the analysis, but found to be only marginally significant. The 0.1% measurement of α_1 is in very good agreement with the most recent calculations. The 20% measurement of α_2 is in fair agreement with calculations.

[1] S. R. Lundeen, in *Advances in Atomic, Molecular, and Optical Physics*, edited by P. R. Berman and C. C. Lin (Academic Press, New York, 2005), Vol. 52, pp. 161–208.
[2] E. S. Chang and R. W. Noyes, Astrophys. J. **275**, L11 (1983).
[3] B. J. Lyons and T. F. Gallagher, Phys. Rev. A **57**, 2426 (1998).
[4] C. S. Wood, S. C. Bennett, D. Cho, B. P. Masterson, J. L. Roberts, C. E. Tanner, and C. E. Wieman, Science **275**, 1759 (1997).
[5] M. S. Safronova and W. R. Johnson, *Advances in Atomic, Molecular, and Optical Physics*, edited by E. Arimondo, P. R. Berman, and C. C. Lin Academic Press, New York, 2008), Vol. 55, pp. 191–233.
[6] E. L. Snow and S. R. Lundeen, Phys. Rev. A **76**, 052505 (2007).
[7] F. J. Deck, E. A. Hessels, and S. R. Lundeen, Phys. Rev. A **48**, 4400 (1993).
[8] E. L. Snow, R. A. Komara, M. A. Gearba, and S. R. Lundeen, Phys. Rev. A **68**, 022510 (2003).
[9] E. L. Snow and S. R. Lundeen, Phys. Rev. A **75**, 062512 (2007).
[10] G. W. F. Drake and R. A. Swainson, Phys. Rev. A **44**, 5448 (1991).
[11] R. A. Komara, M. A. Gearba, S. R. Lundeen, and C. W. Fehrenbach, Phys. Rev. A **67**, 062502 (2003).
[12] M. S. Safronova, W. R. Johnson, and A. Derevianko, Phys. Rev. A **60**, 4476 (1999).
[13] M. Safronova (private communication).
[14] NIST atomic spectra data base, http://physics.nist.gov/PhysRefData/ASD
[15] C. E. Theodosiou, L. J. Curtis, and C. A. Nicolaides, Phys. Rev. A **52**, 3677 (1995).
[16] L. J. Curtis, J. Phys. B **40**, 3173 (2007).
[17] L. J. Curtis (private communication).
[18] L. Hamonou and A. Hibbert, J. Phys. B **40**, 3555 (2007).
[19] J. Mitroy and J. Y. Zhang, Eur. Phys. J. D **46**, 415 (2007).